Available online at www.sciencedirect.com
SCIENCE DIRECT®
International Journal of Plasticity 22 (2006) 1683–1698
INTERNATIONAL JOURNAL OF Plasticity
www.elsevier.com/locate/ijplas

The role of superdislocations for modeling plastic deformation of lamellar TiAl

M. Werwer, A. Cornec *

GKSS Research Centre Geesthacht, Institute for Materials Research, Max-Planck-Strasse 1, 21502 Geesthacht, Germany

Available online 29 March 2006

Abstract

The deformation behaviour of lamellar TiAl-alloys is investigated by means of micromechanical finite element simulations. For the simulations, a lower and an upper bound periodic unit cell representing the lamellar substructure are used. Crystallographic slip is described by continuum crystal plasticity. For the simulations, 16 individual ordinary, super, and twinning systems divided into three morphological slip modes are taken into account. The strength and hardening parameters of the slip systems are determined by comparison with experimental data from room temperature compression tests of poly-synthetically twinned (PST) crystals of TiAl. The effect of the yield stress of the superdislocations is investigated by systematic parameter variations. The results show that the general anisotropy of PST-crystals can already be described with a purely morphological classification of the slip systems. Superdislocations cause a slight tension–compression anomaly if the yield stresses are higher than for the ordinary and twinning systems.

Keywords: A: Lamellar microstructure; B: Crystal plasticity; Polycrystalline material; C: Finite elements; Multiscale model

1. Introduction

TiAl alloys are promising high temperature light-weight structural materials for service temperatures up to 800 °C (Kim and Dimiduk, 1991; Appel and Wagner, 1998; Clemens et al., 1999). The most balanced properties for the desired high temperature applications

* Corresponding author. Tel.: +49 4152 872 535; fax: +49 4152 872 534.
E-mail address: cornec@gkss.de (A. Cornec).

0749-6419/$ - see front matter © 2006 Elsevier Ltd. All rights reserved.
doi:10.1016/j.ijplas.2006.02.005

Notation

α, β	subscript for slip systems
$\dot{\gamma}^{(\alpha)}$	shear rate of slip system α
λ	domain aspect ratio $D_{\mathrm{lam}}/D_{\mathrm{dom}}$
$\tau^{(\alpha)}$	resolved shear (Schmid) stress of slip system α
$g^{(\alpha)}$	flow stress of slip system α
$g_0^{(\alpha)}$	initial yield stress (CRSS) of slip system α
$h_0^{(\alpha)}$	linear hardening modulus of slip system α
m	strain rate exponent
$q_{\alpha\beta}$	hardening matrix
D_{dom}	domain size
D_{lam}	lamellar spacing
Q_{so}	ratio of the yield stress of the superdislocation to the yield stress of the ordinary dislocations: $g_0^{\mathrm{super}}/g_0^{\mathrm{ord}}$
R	relative transverse plastic strain: $R = (\epsilon_{xx}/\epsilon_{yy})_{\mathrm{pl}}$

are achieved with fine grained fine lamellar microstructures (Appel and Wagner, 1998; Kim, 1994; Kim and Dimiduk, 1997; Kim, 1998). Like other intermetallic alloys, lamellar TiAl alloys suffer from poor ductility and fracture toughness. Apparently, one of the reasons for the poor ductility is the complex interaction of the two intermetallic phases with various slip systems of which some are rather sessile and have very high critical resolved shear stresses.

Especially, the superdislocations of the γ-phase seem to play an important role for the deformation behaviour of lamellar TiAl. However, even though there is clear evidence that superdislocations are kinematically necessary for the plastic deformation (Mecking et al., 1996), it is still unclear to which extent they are needed, and, how they do affect the mechanical behaviour of lamellar TiAl.

Micromechanical modelling may help to understand the role of the superdislocations in lamellar microstructures. For TiAl related crystals important micromechanical simulations have been reported by Kad et al. (1995a), Kad et al. (1995b), Parteder et al. (1995), Dao et al. (1996), Kad and Asaro (1997), Schlögl and Fischer (1997a), and Schlögl and Fischer (1997b), and more recently by Brockman (2003), Marketz et al. (2003), and Roos et al. (2004). The focus of the works of Asaro and Brockman, however, was not yet on the interaction of the various dislocations. In their works, the compound of the two phases α_2 and γ is treated as a homogeneous phase where superdislocations are not explicitly considered. The contributions of Fischer and co-workers consider the slip geometry of the α_2 and γ phases and the role of twinning deformation using microstructural representative volume elements (RVEs). Their recent comprehensive investigation considers two basic microstructures as equi-axed near γ-TiAl grains and fully lamellar collonies also for higher temperature and provides substantial aspects of TiAl deformation. However, as polycrystal deformation of lamellar microstructures are modeled by a plane strain approximation in their work, some aspects of the genuine 3D orientation problem might not be reflected appropriately. In the work of Roos et al. (2004) a multiscale modelling is applied based on the transformation field analysis, where the deformation behaviour of different

γ-TiAl microstructures are simulated with morphological slip parameters for the lamellar grains but without considering the parameter effects from superdisocations.

In the present work, we use a systematic approach to investigate the role of the superdislocations. For the micromechanical simulations, we use two different 3D periodic unit cells representing a lower and an upper bound for the mechanical behaviour of the lamellar substructure. The ratio of the yield stress of the superdisloctions to the yield stress of the ordinary dislocations (Q_{so}) is varied systematically. For both unit cells and various Q_{so}-values, parameter sets for the γ slip systems are estimated by comparison with experimental data from PST compression tests. The effect of Q_{so} on the yield behaviour of lamellar TiAl is explored.

2. Microstructure and deformation mechanisms

The lamellar or poly-synthetically twinned (PST) structure of TiAl consists of the two intermetallic phases α_2 and γ with the crystallographic structures $D0_{19}$ and $L1_0$, respectively, Fig. 1(a). There is an orientation relationship between the α_2 and γ platelets. The closely packed planes $(0001)_{\alpha_2}$ and $\{111\}_{\gamma}$, as well as the closely packed directions $\langle 11\bar{2}0\rangle_{\alpha_2}$ and $\langle 1\bar{1}0]_{\gamma}$ are parallel. Six distinct orientation variants of γ fulfil the orientation relationship, Fig. 1(b). These can be distinguished with regard to the stacking order into three matrix-variants and three twin-variants. The γ-lamellae show a domain structure, Fig. 1(c). Within one γ-lamella, the stacking order is nearly constant (Inui et al., 1992a), therefore, γ-matrix and γ-twin lamellae can be distinguished. The lamellar polycrystal, finally, is an assembly of small PST-crystals, as shown in Fig. 1(d).

In the α_2-phase, $\langle 11\bar{2}0\rangle$ $\{1\bar{1}00\}$ prismatic and to a lesser extent $\langle 11\bar{2}0\rangle$ (0001) basal, and $\langle\bar{1}\bar{1}26\rangle$ $\{11\bar{2}1\}$ pyramidal slip systems are observed, Fig. 2(a). The critical resolved shear stresses (CRSS) of the α_2 slip systems have been estimated from α_2 single crystals (Minonishi, 1991; Umakoshi et al., 1993a; Umakoshi et al., 1993b; Inui et al., 1993). For the simulations, we used the values reported in Inui et al. (1993) (prism: 100 MPa, basal: 300 MPa, pyramidal: 910 MPa). Even though in lamellar TiAl the α_2-slip systems are likely to be stronger due to the impurities concentrated in this phase, these values may serve as a first estimate.

In the γ-phase, slip predominantly occurs by $1/2\langle 1\bar{1}0]$[1] $\{111\}$ ordinary dislocations, $1/6\langle 11\bar{2}]$ $\{111\}$ partial dislocations responsible for twinning, and to a lesser extent by $1/2\langle 11\bar{2}]$ $\{111\}$ and $\langle 10\bar{1}]$ $\{111\}$ superdislocations (Kishida et al., 1998). For the sake of simplicity, we have neglected the $1/2\langle 11\bar{2}]$ superdislocations. The additional effect of these superdislocations on the simulation of the deformation behaviour is small, since the same deformation can be achieved with a combination of a $1/2\langle 1\bar{1}0]$ ordinary with a $\langle 10\bar{1}]$ superdislocation.

Until now, the CRSS have not experimentally been determined for a γ-phase in equilibrium with α_2. Experiments have only been performed on γ-single crystals with an aluminium concentration of 54% or 56% (e.g., Kawabata et al., 1990; Inui et al., 1997). In two-phase alloys, the estimation of the CRSS of the γ-phase is complicated by the lamellar morphology. In the lamellar compound, the free slip length of the dislocations is limited by the lamellae dimensions. The effective CRSS of the slip systems may therefore depend on

[1] The mixed notation $\langle u\,v\,w]$ denotes permutations $\pm u$, $\pm v$, w.

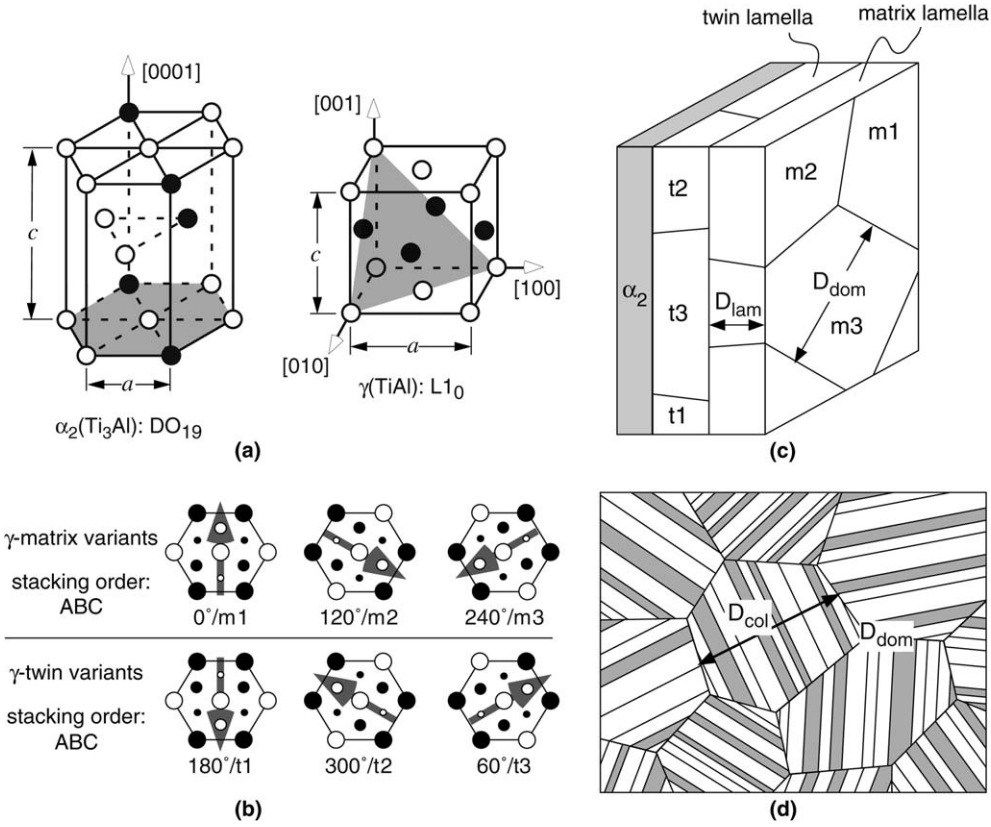

Fig. 1. Microstructure of lamellar TiAl: (a) crystallographic structures of α_2 and γ; (b) orientation variants of γ; (c) lamellar (PST) substructure; (d) polycrystal (colony) structure.

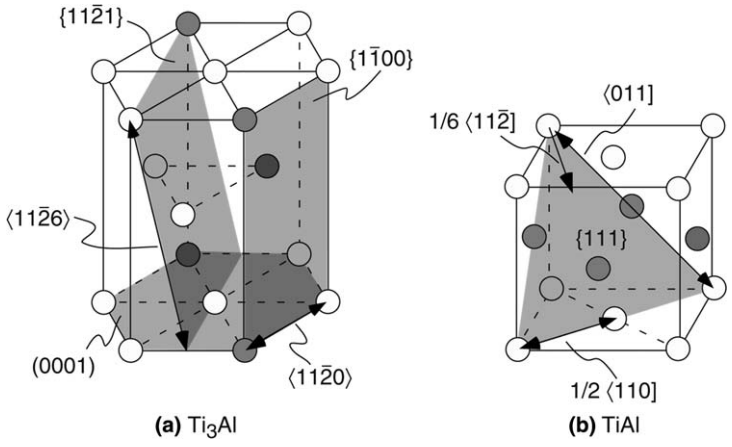

Fig. 2. Slips systems: (a) of the α_2-phase; (b) of the γ-phase.

the orientation of the slip systems relative to the lamellar boundary. Generally, the γ slip systems can morphologically be divided into three slip modes:

- Longitudinal mode: glide on longitudinal {1 1 1}-planes (parallel to the interface), Fig. 3(a).
- Mixed mode: glide on transverse {1 1 1}-planes (inclined to the lamellar boundary) in longitudinal directions, Fig. 3(b).
- Transverse mode: glide on transverse {1 1 1}-planes in transverse directions, Fig. 3(c).

For the simulations, the γ-phase slip systems were classified morphologically and crystallographically, Table 1. Totally eight classes of γ-phase slip systems can be distinguished for which different slip and hardening parameters can be assumed.

3. Modelling

3.1. Crystal plasticity

The deformation behaviour of the α_2- and the γ-phases is described by continuum crystal plasticity (Asaro, 1983), which describes the shear deformation of a solid due to glide of dislocations obeying the Schmid-law. A modified version of the ABAQUS user defined material subroutine (UMAT) originally developed by Huang (1991) was used for the simulations.

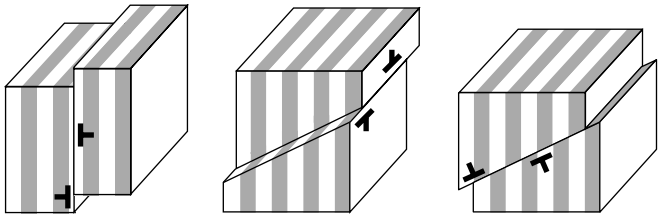

Fig. 3. Morphological classification of the slip systems in a PST crystal: (a) longitudinal mode; (b) mixed mode; (c) transverse mode.

Table 1
Classification of the γ slip systems

Classification	Longitudinal	Mixed	Transverse
Ordinary	$1/2[1\,\bar{1}\,0]\ (1\,1\,1)$	$1/2[1\,\bar{1}\,0]\ (1\,1\,\bar{1})$	$1/2[1\,1\,0]\ (1\,\bar{1}\,1)$
	–	–	$1/2[1\,1\,0]\ (1\,\bar{1}\,\bar{1})$
Super	$[0\,1\,\bar{1}]\ (1\,1\,1)$	$[0\,1\,\bar{1}]\ (1\,\bar{1}\,\bar{1})$	$[0\,\bar{1}\,\bar{1}]\ (1\,1\,\bar{1})$
	$[1\,0\,\bar{1}]\ (1\,1\,1)$	$[1\,0\,\bar{1}]\ (1\,\bar{1}\,1)$	$[\bar{1}\,0\,\bar{1}]\ (1\,1\,\bar{1})$
	–	–	$[0\,\bar{1}\,\bar{1}]\ (1\,\bar{1}\,1)$
	–	–	$[\bar{1}\,0\,\bar{1}]\ (1\,\bar{1}\,\bar{1})$
Twinning	$1/6[1\,1\,\bar{2}]\ (\bar{1}\,\bar{1}\,\bar{1})$	–	$1/6[\bar{1}\,\bar{1}\,\bar{2}]\ (1\,1\,\bar{1})$
	–	–	$1/6[\bar{1}\,1\,\bar{2}]\ (\bar{1}\,1\,\bar{1})$
	–	–	$1/6[\bar{1}\,1\,\bar{2}]\ (1\,\bar{1}\,\bar{1})$

The constitutive law used in the UMAT is based on a rate-dependent visco-plastic formulation:

$$\frac{\dot{\gamma}^{(\alpha)}}{\dot{\gamma}_0} = \left|\frac{\tau^{(\alpha)}}{g^{(\alpha)}}\right|^{m-1}\left(\frac{\tau^{(\alpha)}}{g^{(\alpha)}}\right), \tag{1}$$

where $\dot{\gamma}^{(\alpha)}$ is the shear rate of the slip system α, $\dot{\gamma}_0$ is a reference shear rate, $\tau^{(\alpha)}$ is the Schmid-stress in α, $g^{(\alpha)}$ is the flow stress of α, and m is the strain rate exponent.

The evolution of $g^{(\alpha)}$ is described by a linear hardening law:

$$\dot{g}^{(\alpha)} = h_0^{(\alpha)} \sum_{\beta} q_{\alpha\beta}\dot{\gamma}^{(\beta)}, \tag{2}$$

where $h_0^{(\alpha)}$ is the hardening modulus, and $q_{\alpha\beta}$ is the hardening matrix. The values of $q_{\alpha\beta}$ are generally found to be in the range of 1.0–1.4. Until now, there are no experimental estimates of $q_{\alpha\beta}$ either for α_2 and γ. Therefore, we did not distinguish self and latent hardening and assumed $q_{\alpha\beta} = 1.0$ for all slip systems α and β.

Twinning is implemented in the UMAT as unidirectional glide of the $1/6\langle 1\,1\,\bar{2}]$ partial dislocations. The unidirectionality of the twinning dislocations is enforced numerically. The crystallographic reorientation due to twinning is neglected.

For the simulations, the slip systems are characterized by the initial yield stresses $g_0^{(\alpha)}$, which are essentially identical with the CRSS, and the hardening moduli $h_0^{(\alpha)}$. In order to reduce the number of free parameters, the slip parameters of the ordinary and twinning dislocations were characterized morphologically by the yield stresses g_0^{long}, g_0^{mix} and g_0^{trans}. The yield stresses of the superdislocations were characterized by the ratio of the yield stress of the superdislocations to the yield stress of the ordinary dislocations Q_{so}. The hardening parameters were characterized by h_0^{long}, h_0^{mix} and h_0^{trans}.

3.2. Periodic unit cells

The deformation behaviour of the lamellar compound is described by periodic unit cells. From a continuum-mechanical point of view, the deformation behaviour of a solid does not depend on absolute length scales like the lamellar spacing D_{lam} and the domain size D_{dom}. The behaviour may, however, depend on the relative length scales. In the lamellar substructure, there is only one relative length scale to be considered, which is the domain aspect ratio $\lambda = D_{\text{lam}}/D_{\text{dom}}$. With regard to λ, two limits can be distinguished:

In the case of $\lambda \to 0$, the domains can be treated as individual lamellae. A geometric representation for this case is the periodic unit cell RVE7 which consists of one α_2-lamella, three γ-matrix-lamellae (m1–m3) and three γ-twin lamellae (t1–t3). In the finite element (FE) model, each lamella is represented by a single FE element, Fig. 4(a).

In the case of $\lambda \to \infty$, the deformation within a γ-lamella is uniform. This assumption is represented by the unit cell RVE9. The FE-model of RVE9 consists totally of nine FE-elements: three α_2-elements, three γ-matrix elements (m1–m3), and three γ-twin elements (t1–t3), Fig. 4(b). The uniform deformation of the three matrix-domains and the three twin-domains is enforced by appropriate constraint equations.

Regarding the interlamellar deformation, the unit cells RVE7 and RVE9 represent a statically admissible stress field and a kinematically admissible strain field, respectively. According to the limit load theorems of plasticity (Prager, 1952), RVE7 and RVE9 mark lower and upper bounds for the intralamellar yield stress. The yield stress of all other

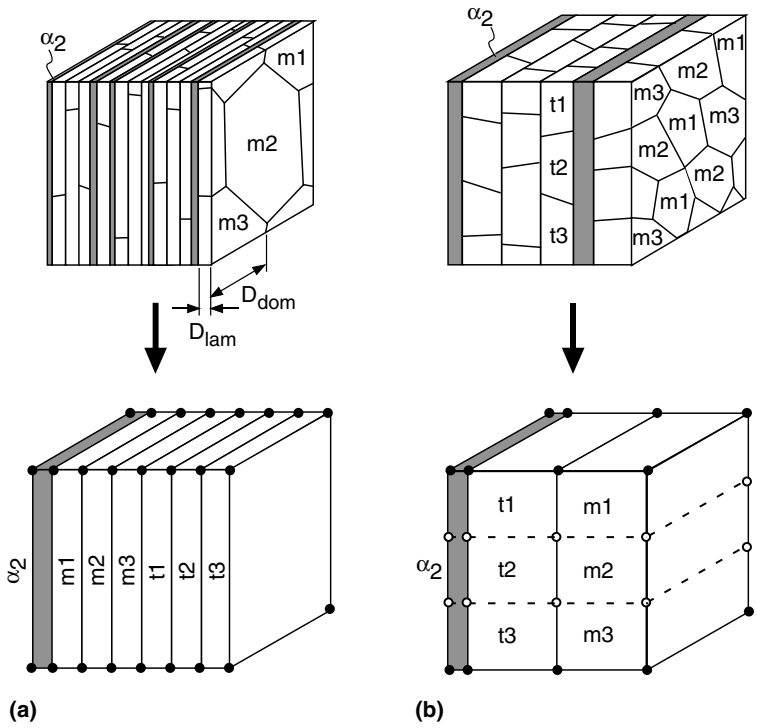

Fig. 4. Unit-cells representing the lamellar (PST) substructure: (a) small domian aspect ratio (RVE7); (b) large domain aspect ratio (RVE9).

geometric representations of the intralamellar structure, e.g., the one used by Parteder et al. (1995) and Schlögl and Fischer (1997a,b), lies between these two bounds.

Due to the periodic boundary conditions, any arbitrary deformation can be applied to periodic unit cells (Werwer and Cornec, 2000). Therefore, simulations of the lamellar substructure can be performed for arbitrary lamellar orientations φ with respect to the loading axis without any internal changes of the unit cells. An application of the unit cell aproach to lamellar TiAl polycrystals is described by Cornec et al. (2003).

4. Results

For estimating the slip parameters of the γ-phase, compression tests on PST-crystals, performed by Uhlenhut (1999), were simulated with the periodic unit cells RVE7 and RVE9. The chemical composition of the PST-crystals was Ti–49.3 mol% Al. The lamellar spacing was $D_{\mathrm{lam}} \approx 2$ μm.

The first parameter sets were estimated for $Q_{\mathrm{so}} = 1.0$. The slip and hardening parameters estimated for RVE7 are listed in Table 2 (set #7.1), and for RVE9 in Table 3 (#9.1). With $Q_{\mathrm{so}} = 1.0$, the parameter estimation yields the same parameters for RVE7 and RVE9. Fig. 5(a) shows the calibrated yield curves and the experimental data for the orientations $\varphi = 0°$, 45° and 90°. For both unit cells, the experimental yield curves are excellently matched up to high strains of 15%. Especially for the 90° orientation, the initial

Table 2
Sip parameter of the γ-phase estimated for RVE7

Set	Q_{so}	g_0^{long} (MPa)	g_0^{mixed}	g_0^{trans} (MPa)	h_0^{long} (MPa)	h_0^{mixed} (MPa)	h_0^{trans} (MPa)
RVE7.1	1.0	55	150	185	400	320	135
RVE7.∞	∞	55	150	185	400	320	135
RVE7.2	2.0	45	85	150	310	350	180
RVE7.5	5.0	45	40	155	235	320	150

Table 3
Sip parameter of the γ-phase estimated for RVE9

Set	Q_{so}	g_0^{long} (MPa)	g_0^{mixed}	g_0^{trans} (MPa)	h_0^{long} (MPa)	h_0^{mixed} (MPa)	h_0^{trans} (MPa)
RVE9.1	1.0	55	150	185	400	320	135
RVE9.∞	∞	55	150	185	400	320	135
RVE9.2	2.0	35	90	125	350	350	90
RVE9.5	5.0	22	45	120	300	360	50

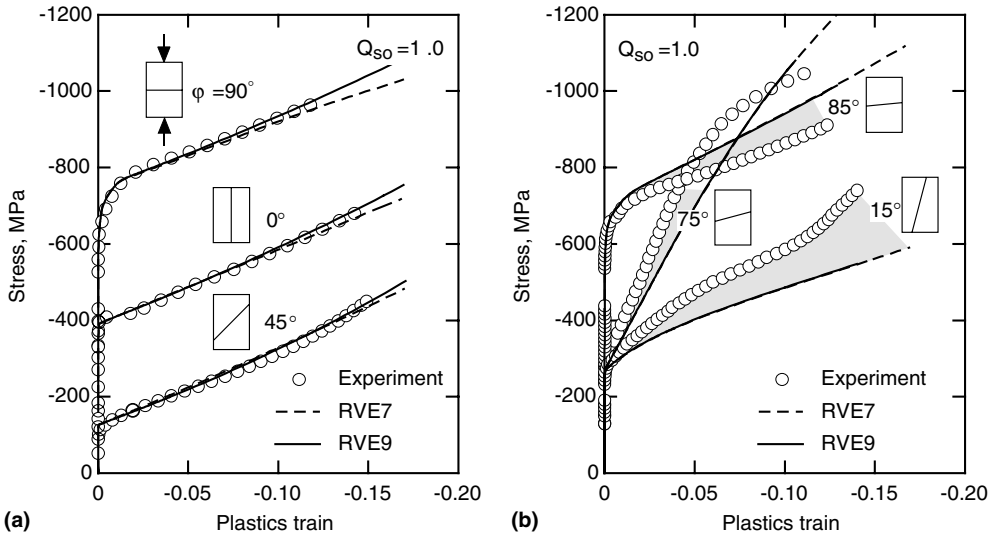

Fig. 5. Flow stress curves of PST-crystals in compression for various orientations φ. Simulations of RVE7 and RVE9 using a purely morphological parameter set and comparison with experimental data: (a) $\varphi = 0°$, 45°, and 90°; (b) $\varphi = 15°$, 75°, and 85°.

transient regime in the yield curve is correctly reflected although a linear hardening law was assumed for the slip systems. Fig. 5(b) shows the yield curves for the orientations 15°, 75°, and 85°. The unit cells RVE7 and RVE9 give essentially the same yield curves. The simulations match the experimental data reasonably well. Especially for the 75° orientation, the strong work hardening behaviour due to the crystallographic rotation is qualitatively well reflected. There are, however, quantitative differences in the hardening behaviour. These may be explained by the inhomogeneous deformation occuring in the experiments but not in the simulations, which always represent perfectly homogeneous conditions.

For investigating the kinematical necessity of the $\langle 0\,1\,1]$ superdislocations, tension and compression yield curves were calculated with the same parameters for the ordinary and twinning systems, however, the glide of superdislocations was suppressed ($Q_{so} \to \infty$).

For RVE7, Fig. 6(a) and (b) shows the effect of the suppression of the superdislocations for the PST-orientations 0°, 45°, and 90°. Without superdislocations, the 0°-orientation in compression and the 90°-orientation in tension show an anomalous strong hardening. Apparently, superdislocations are kinematically necessary for these two load cases. All the other load cases show a normal hardening behaviour even without superdislocations.

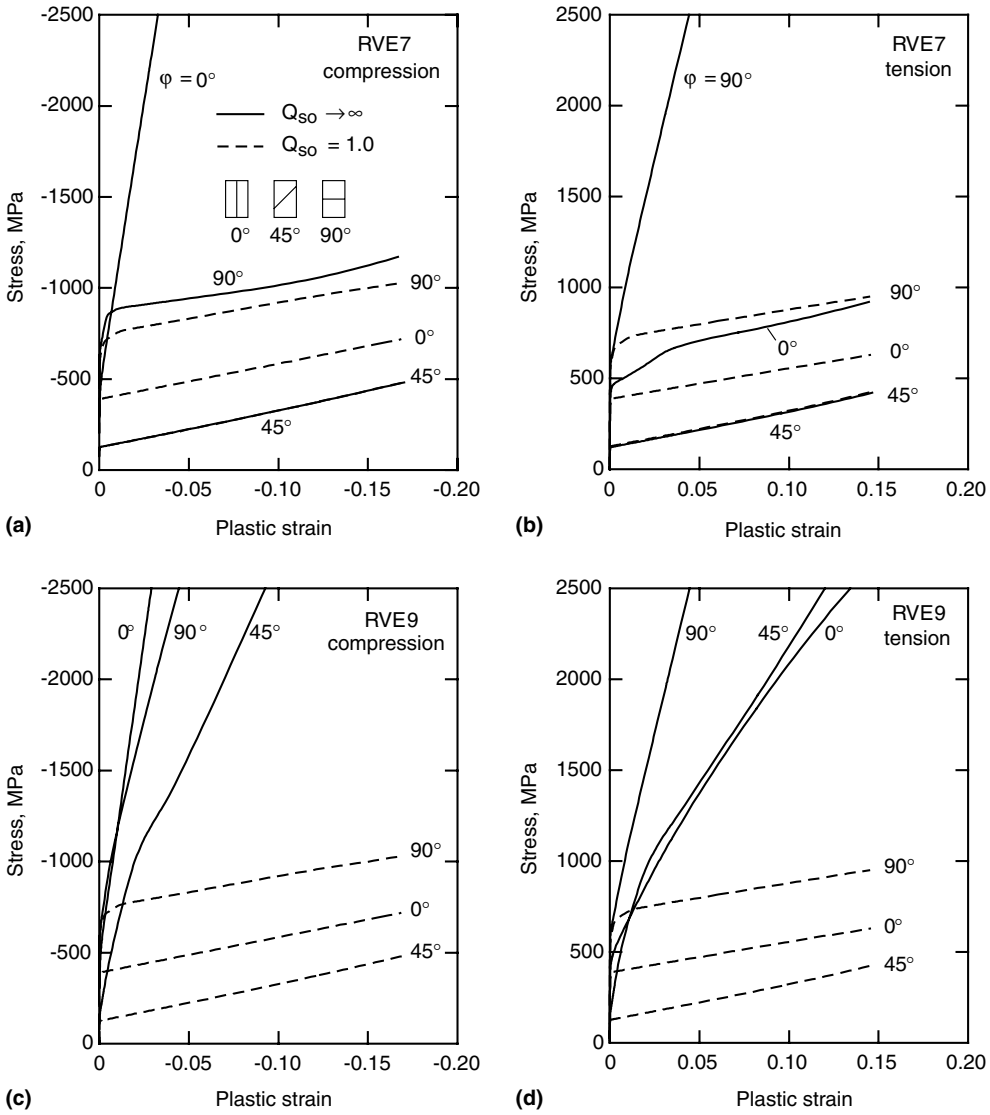

Fig. 6. Effect of the suppression of the superdislocations on the PST yield curves: (a) RVE7-compression; (b) RVE7-tension; (c) RVE9-compression; RVE9-tension.

For RVE9, Fig. 6(c) and (d) shows the compression and tensile yield curves with suppressed super slip. For this unit cell, apparently, superdislocations are kinematically necessary for all load cases.

The parameter estimation was repeated for $Q_{so} = 2.0$ and 5.0. The parameters are listed in Tables 2 and 3, respectively. Fig. 7 shows for both unit cells the yield curves fitted to the experimental data. For all Q_{so}-values a parameter set can be found which matches the experimental data very well. For the 90°-orientation, however, the unit cell RVE9 does not accurately reflect the linear hardening behaviour after the initial transition regime if $Q_{so} > 1.0$.

Fig. 8 shows the yield stresses estimated for the superdislocations dependent on Q_{so}. For RVE7, the yield stress of the longitudinal and transverse superdislocations increases without limit. Apparently, these dislocations can be bypassed by combinations of other slip systems. Therefore, they are kinematically not necessary. In contrast, the yield stress of the mixed mode superdislocations approaches a value of approximately 200 MPa. These dislocations are kinematically necessary.

For RVE9, the yield stress estimated for the transverse superdislocations increases without limit, while the yield stress estimated for the longitudinal and mixed mode superdislocations approaches asymptotically finite values. Apparently, the transverse superdislocations can be bypassed by other dislocations. The longitudinal and transverse slip systems, however, are kinematically necessary.

Due to the unidirectionality of twinning, TiAl may show a tension–compression anomaly. As an example, the tension–compression anomaly was investigated with the unit cell RVE7 for the 0°-PST-orientation.

Fig. 9(a) shows the tension–compression yield stress anomaly expressed by the ratio of the compressive yield stress to the tensile yield stress versus Q_{so}. For $Q_{so} = 1.0$ the simulation does essentially not show a tension–compression anomaly. The compression–

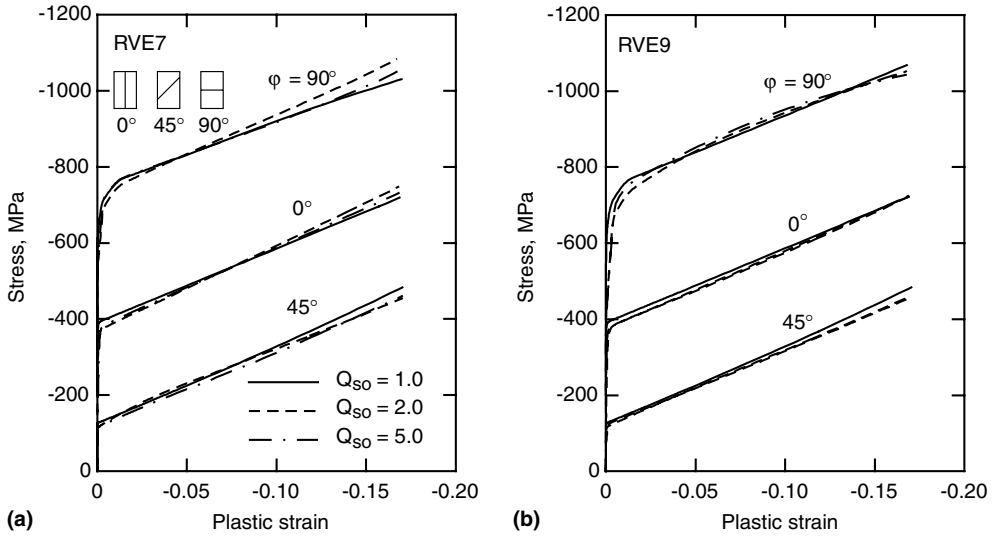

Fig. 7. Recalculated PST-yield curves under compression for various Q_{so}-values: (a) calculated with RVE7, (b) calculated with RVE9. The actual experimental data can be found in Fig. 5.

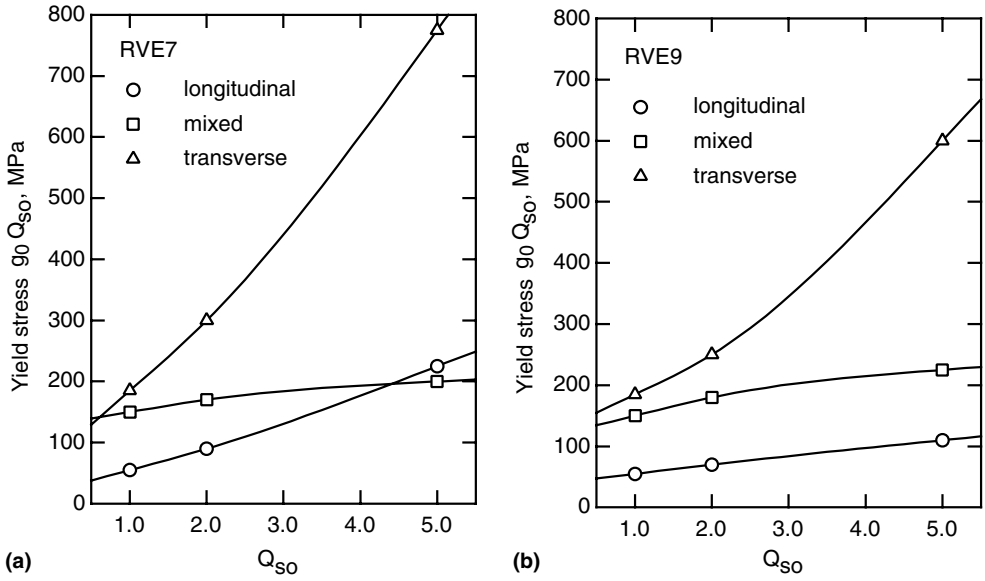

Fig. 8. Yield stresses of the superdislocations estimated for various Q_{so}: (a) for RVE7, (b) for RVE9.

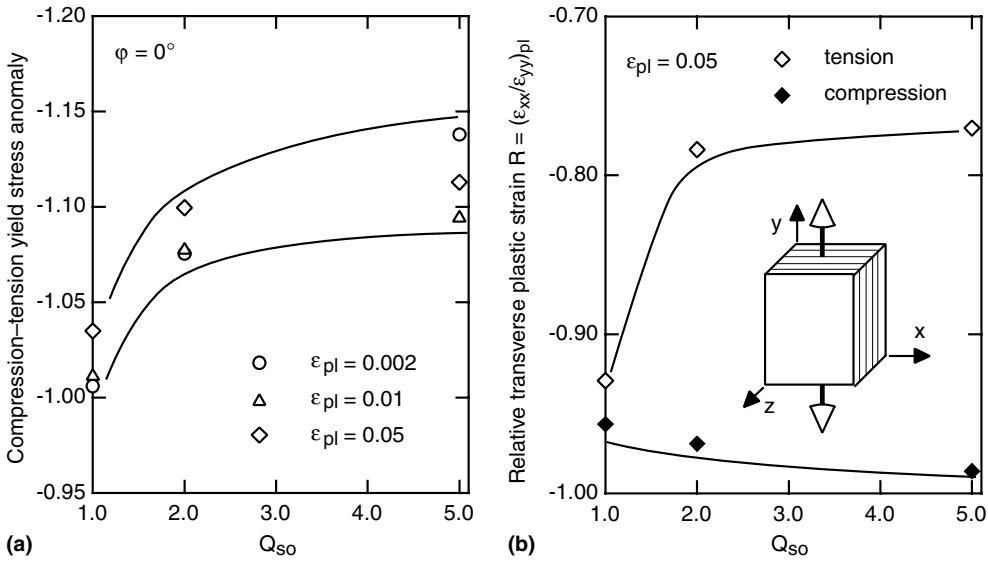

Fig. 9. Effect of the super/ordinary strength ratio: (a) tension/compression anomaly; (b) relative plastic transverse strains.

tension yield stress anomaly increases slightly with increasing Q_{so} with a slight dependence of the strain level. For high Q_{so}-values, the compressive yield stress is approximately 10–15% higher than the tensile yield stress.

Fig. 9(b) shows the tension–compression anomaly of the relative plastic transverse strains expressed by $R = (\epsilon_{xx}/\epsilon_{yy})_{pl}$. In compression, the simulation shows a plane strain

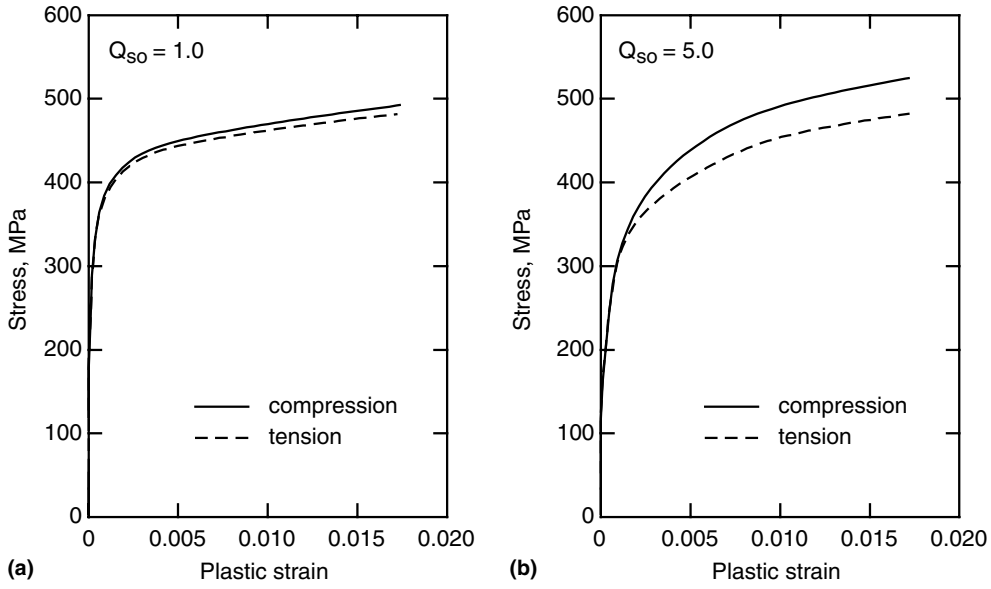

Fig. 10. Polycrystal yield curves simulated with the Taylor-model using 64 unit cells RVE7: (a) $Q_{so} = 1.0$; (b) $Q_{so} = 5.0$.

deformation without reduction of the lamellar spacing ($R = -1.0$). In tension, the simulation shows the plane strain deformation only for $Q_{so} = 1.0$. For $Q_{so} > 1.0$, a value of $R = -0.8$ is found.

Finally, polycrystal simulations were performed with the Taylor-Model (Taylor, 1938). For the polycrystal simulations, 64 unit cells (RVE7) with a quasi-isotropic random orientation distribution were used.

Fig. 10 shows the compressive and tensile yield curves estimated for the parameter sets RVE7.1 ($Q_{so} = 1.0$) and RVE7.5 ($Q_{so} = 5.0$), see Table 2. For the parameter set RVE7.1, the simulation shows essentially the same behaviour in tension and compression. For the parameter set RVE7.5, however, the yield stress is in compression significantly higher than in tension. Furthermore, the initial transient regime of the yield curve is more pronounced with set RVE7.5 than with RVE7.1.

5. Discussion

Micromechanical modelling has become increasingly popular since modern computers provide enough computational power for the complex simulations. Currently, there is no lack of micromechanical models. The essential point of micromechanical modelling, however, is not to develop new or more complex models, but the estimation of the free model parameters. Frequently, there are more parameters hidden in the models than there is relevant characteristic data from the experiments. This makes it sometimes difficult to draw useful conclusions from micromechanical simulations.

In this work, we proposed a lower bound (RVE7) and an upper bound (RVE9) unit cell for the simulation of the co-deformation of the various constituents present in lamellar TiAl (α_2, six different γ-orientation variants). As a first approximation, we assumed a

purely morphological set of γ-phase slip parameters ($Q_{so} = 1.0$). This parameter set contains three yield parameters ($g_0^{long}, g_0^{mixed}, g_0^{trans}$) and three hardening parameters ($h_0^{long}, h_0^{mixed}, h_0^{trans}$). These can uniquely be estimated from PST-compression tests with the orientations 0°, 45° and 90°. For the PST-material investigated, we found the values $g_0^{mixed} : g_0^{long} = 2.72$ and $g_0^{trans} : g_0^{long} = 3.27$. These values agree excellently with the findings of Lebensohn et al. (1998). With the purely morphological parameter set, the yield curves of all other PST-orientations can be simulated with a reasonable accuracy up to strains of 15%. In contrast, other micromechanical models (e.g., Schlögl and Fischer, 1997b; Brockman, 2003), just reflect the orientation dependence of the initial yield stress.

From TEM investigations on lamellar TiAl, there is a clear evidence that $\langle 0\,1\,1]$ superdislocations are significantly stronger than $1/2\langle 1\,1\,0]$ ordinary and $1/6\langle 1\,1\,\bar{2}]$ twinning dislocations (Appel and Wagner, 1998; Kishida et al., 1998). The assumption of a purely morphogical parameter set is therefore not in accordance with the experimental evidence. To investigate the effect of the superdislocations, the yield stress ratio $Q_{so} = g_0^{super}/g_0^{ord}$ was introduced as an additional parameter. Since the characteristic experimental data from the PST-compression tests is already used for the estimation of the g_0- and h_0-values, however, the parameter Q_{so} cannot directly be estimated from the PST-compression test data.

Generally, $1/2\langle 1\,1\,0]$ ordinary and $1/6\langle 1\,1\,\bar{2}]$ twinning slip systems do not provide five independent slip systems. Therefore, superdislocations are kinematically necessary for a general deformation of lamellar TiAl (Mecking et al., 1996). However, the $\langle 0\,1\,1]$ superdislocations are not required for all deformation modes. To investigate which deformation modes do not require the activation of $\langle 0\,1\,1]$ superdislocations, the case $Q_{so} \to \infty$ was considered.

For the lower bound unit cell RVE7, the $\langle 0\,1\,1]$ superdislocations are kinematically necessary for the load cases 0°-compression and 90°-tension, while for all other load cases the superdislocations can be bypassed. For the upper bound unit cell RVE9, the $\langle 0\,1\,1]$ superdislocations are kinematically necessary for all load cases. Theoretically, the behaviour of a fine lamellar alloy (with a small domain aspect ratio) should be closer to RVE7 while the behaviour of a coarse lamellar alloy (with a high domain aspect ratio) should be closer to RVE9.

For a finite value of Q_{so}, the PST compression tests can be simulated by the unit cells RVE7 and RVE9. The accuracy, however, seems to be slightly better for the unit cell RVE7. It seems, therefore, that RVE7 is the more appropriate model when compared with RVE9.

Since twinning is a unidirectional process, the deformation modes which do not require the activation of superdislocations are not the same in tension and compression. This effect may introduce a tension–compression anomaly for $Q_{so} > 1.0$. We investigated the tension–compression anomaly in an exemplary way for the unit cell RVE7. The yield stress, however, shows only a slight tension compression anomaly. The compressive yield stress may be 10–15% higher than the tensile yield stress if the superdislocations are very strong. Experimentally, the tension–compression anomaly of PST-crystals was investigated by Inui et al. (1992b). In this work, no significant tension–compression anomaly was found. However, the scatter for such experiments is usually in the same order of magnitude as the tension–compression anomaly estimated by our simulation. From Inui's experimental data, it is therefore not possible to conclude evidently on the strength of the superdislocations.

Besides the yield stress, also the relative plastic transverse strains show a tension–compression anomaly. According to our simulations, the 0°-PST-orientation shows in compression a plane strain deformation without reduction of the lamellar spacing

($R = -1.0$). In tension, however, a value of $R = -0.8$ is found in the case of strong superdislocations. Experimentally, the tension–compression anomaly of the relative plastic strains was investigated by Kishida et al. (1998). They found $R = -1.0$ for compression, and $R = -0.67$ for tension. These values are qualitatively in good agreement with our results. The monitoring of the transverse strains during the experiments might therefore provide additional characteristic data for the estimation of the strength of the superdislocations.

A slight tension–compression anomaly of the yield stress is also found for the polycrystal simulation. Experimentally, there is a weak evidence of a tension–compression anomaly present in lamellar TiAl-polycrystals at high temperature (Schillinger et al., 2002; Wu et al., 2002). This might indicate that the superdislocations become increasingly strong at higher temeratures. However, for a clearer picture of the tension–compression anomaly of lamellar TiAl more experimental evidence is needed.

6. Conclusions

The role of the superdislocations for the room temperature deformation behaviour of TiAl PST crystals was investigated by means of periodic unit cells simulations. The results obtained may be summarized as follows.

The plastic anisotropy of PST crystals can be accurately described with the periodic unit cells. The ratio of the yield stress of the superdislocations to the yield stress of the ordinary dislocations, however, cannot uniquely be determined from compression tests on PST crystals.

Superdislocations are kinematically necessary for, at least, certain deformation modes of PST crystals. The extent to which superdislocations are necessary depends on the intralamellar domain structure. The higher the domain aspect ratio, the lower the degrees to which superdislocations are necessary.

Experimentally, there is some evidence that superdislocations in lamellar TiAl are stronger than ordinary and twinning dislocations (e.g., Kishida et al., 1998; Lebensohn et al., 1998), however, if the superdislocations were significantly stronger, the PST crystals as well as the lamellar TiAl polycrystals should show a slight tension–compression anomaly.

For modeling polycrystal deformation, the presented PST crystal study can be used as an RVE representing the lamellar collonies depending on their individual 3D orientations.

Acknowledgements

The financial support of this work by the German Science Foundation DFG within the collaborative research centre SFB 371 on "Micromechanics of Multiphase Materials" is gratefully acknowledged. Furthermore, the authors thank Henning Uhlenhut for providing the experimental data, and Fritz Appel for helpful discussions.

References

Appel, F., Wagner, R., 1998. Microstructure and deformation of two-phase γ-titanium aluminides. Materials Science and Engineering R22, 187–268.

Asaro, R.J., 1983. Micromechanics of crystals and polycrystalsAdvances in Applied Mechanics, vol. 23. Academic Press, New York, pp. 1–115.

Brockman, R.A., 2003. Analysis of elastic–plastic deformation in TiAl polycrystals. International Journal of Plasticity 19, 1749–1772.

Clemens, H., Lorich, A., Eberhardt, N., Glatz, W., Knabl, W., Kestler, H., 1999. Technology, properties and applications of intermetallic γ-TiAl based alloys. Zeitschrift Metallkunde 90, 569–580.

Cornec, A., Werwer, M., Heitmann, V., 2003. Micromechanical modelling of deformation and fracture in lamellar γ-TiAl-alloys. In: Kim, Y.-W., Clemens, H., Rosenberger, A. (Eds.), Gamma Titanium Aluminides 2003. The Minerals, Metals and Materials Society (TMS), Warrendale, pp. 493–501.

Dao, M., Kad, B.K., Asaro, R.J., 1996. Deformation and fracture under compressive loading in lamellar TiAl microstructures. Philosophical Magazine A 74, 569–591.

Huang, Y., 1991. A user-material subroutine incorporating single crystal plasticity in the ABAQUS finite element program. Report MECH-178, Division of Applied Science, Havard University, Cambridge, MA.

Inui, H., Oh, M.H., Nakamura, A., Yamaguchi, M., 1992a. Ordered domains in TiAl coexisting with Ti_3Al in the lamellar structure of Ti-rich TiAl compounds. Philosophical Magazine A 66, 539–555.

Inui, H., Oh, M.H., Nakamura, A., Yamaguchi, M., 1992b. Room-temperature tensile deformation of polysynthetically twinned (PST) crystals of TiAl. Acta Metallurgica et Materialia 40, 3095–3104.

Inui, H., Matsumuro, M., Wu, D.-H., Yamaguchi, M., 1997. Temperature dependence of yield stress, deformation mode and deformation structure in single crystals of TiAl (Ti–56 at.% Al). Philosophical Magazine A 74, 395–423.

Inui, H., Toda, Y., Yamaguchi, M., 1993. Plastic deformation of single crystal of a DO_{19} compound with an off-stoichiometric composition (Ti–36.5 at.% Al) at room temperature. Philosophical Magazine A 67, 1315–1332.

Kad, B.M., Asaro, R.J., 1997. Apparent Hall–Petch effects in polycrystalline lamellar TiAl. Philosophical Magazine A 75, 87–104.

Kad, B.M., Dao, M., Asaro, R.J., 1995a. Numerical simulations and fracture effects in two phase γ-TiAl + α_2–Ti_3Al lamellar microstructures. Philosophical Magazine A 71, 567–604.

Kad, B.M., Dao, M., Asaro, R.J., 1995b. Numerical simulations of stress–strain behavior in two-phase $\alpha_2 + \gamma$ TiAl alloys. Materials Science and Engineering A192/193, 97–103.

Kawabata, T., Abumiya, T., Kanai, T., Izumi, O., 1990. Mechanical properties and dislocation structures of TiAl single crystals deformed at 4.2–293 K. Acta Metallurgica et Materialia 38, 1381–1393.

Kim, Y.-W., 1994. Ordered intermetallic alloys, part III: gamma titanium aluminides. Journal of Materials 47 (7), 30–39.

Kim, Y.-W., 1998. Strength and ductility in TiAl alloys. Intermetallics 6, 623–628.

Kim, Y.-W., Dimiduk, D.M., 1991. Progress in understanding of gamma titanium aluminides. Journal of Materials 43 (8), 40–47.

Kim, Y.-W., Dimiduk, D.M., 1997. Designing gamma TiAl alloys: fundamentals, strategy and production. In: Nathal, M.V., Darolia, C.T., Martin, P.L., Miracle, D.B., Wagner, R., Yamaguchi, M. (Eds.), Structural Intermetallics 1997. The Minerals, Metals and Materials Society (TMS), Warrendale, pp. 531–543.

Kishida, K., Inui, H., Yamaguchi, M., 1998. Deformation of lamellar structure in TiAl–Ti_3Al two-phase alloys. Philosophical Magazine A 78, 1–28.

Lebensohn, R., Uhlenhut, H., Hartig, C., Mecking, H., 1998. Plastic flow of γ-TiAl-based polysynthetically twinned crystals: micromechanical modeling and experimental validation. Acta Materialia 46, 4701–4709.

Marketz, W.T., Fischer, F.D., Clemens, H., 2003. Deformation mechanisms in TiAl intermetallics – experiments and modeling. International Journal of Plasticity 19, 281–321.

Mecking, H., Hartig, C., Kocks, U.F., 1996. Deformation modes in γ-TiAl as derived from single crystal yield surface. Acta Materialia 44, 1309–1321.

Minonishi, Y., 1991. Plastic deformation of single crystals of Ti_3Al with $D0_19$ structure. Philosophical Magazine A 63, 1085–1091.

Parteder, E., Siegmund, T., Fischer, F.D., Schlögl, S., 1995. Numerical simulation of the plastic behaviour of polysynthetically twinned Ti–Al crystals. Materials Science and Engineering A192/193, 149–154.

Prager, W., Drucker, D.C., Greenberg, H.J.G., 1952. Extended limit design theorems for continuous media. Quaterly of Applied Mathematics 9, 381–389.

Roos, A., Chaboche, J.-L., Gélébart, L., Crépin, J., 2004. Multiscale modelling of titanium aluminides. International Journal of Plasticity 20, 811–830.

Schillinger, W., Lorenzen, B., Bartels, A., 2002. Anisotropic mechanical behaviour of textures γ-TiAl caused by the directionality of twinning. Materials Science and Engineering A329–A331, 644–648.

Schlögl, S.M., Fischer, F.D., 1997a. Numerical simulation of yield loci for PST crystals of TiAl. Materials Science and Engineering A239–A240, 790–803.

Schlögl, S.M., Fischer, F.D., 1997b. The role of slip and twinning in the deformation behaviour of polysynthetically twinned crystals of TiAl: a micromechanical model. Philosophical Magazine A 75, 621–636.

Taylor, G., 1938. Analysis of plastic strain in a cubic crystal. Journal of Institutional Metals 62, 307–324.

Uhlenhut, H., 1999. Ursachen plastischer anisotropie von γ-TiAl-basislegierungen. Ph.D. Thesis, Technical University of Hamburg, Harburg.

Umakoshi, Y., Nakano, T., Sumimoto, K., Maeda, Y., 1993a. Plastic anisotropy of Ti_3Al single crystals. In: Baker, I., Darolia, R., Whittenberger, J.D., Yoo, M.H. (Eds.), High-temperature Ordered Intermellic Alloys V. Materials Research Society Symposium Proceedings. vol. 288.

Umakoshi, Y., Nakano, T., Takenaka, T., Sumimoto, K., Yamane, T., 1993b. Orientation and temperature dependence of yield stress and slip geometry of Ti_3Al and Ti_3Al–V single crystals. Acta Metallurgica et Materialia 41, 1149–1154.

Werwer, M., Cornec, A., 2000. Numerical simulation of plastic deformation and fracture in polysynthetically twinned (PST) crystals of TiAl. Computational Materials Science 19, 97–107.

Wu, X., Song, D., Xia, K., 2002. Different tensile and compressive creep behaviour in a fully lamellar (Ti–44Al–1Mn–2.5Nb–0.15Gd) alloy. Materials Science and Engineering A329–A331, 821–827.